Author/s:
Momeni, A;McQuillan, RV;Anisi, H;Alivand, MS;Zavabeti, A;Stevens, GW;Kim, S;Mumford, KA

Title:
Catalytic Membrane Vacuum Regeneration: Enhancing Energy Efficiency and Renewable Compatibility in Direct Air Capture

Date:
2025-06-26

Citation:
Momeni, A., McQuillan, R. V., Anisi, H., Alivand, M. S., Zavabeti, A., Stevens, G. W., Kim, S. & Mumford, K. A. (2025). Catalytic Membrane Vacuum Regeneration: Enhancing Energy Efficiency and Renewable Compatibility in Direct Air Capture. Small, 21 (25), pp.e2503023-. https://doi.org/10.1002/smll.202503023.

Persistent Link:
https://hdl.handle.net/11343/362688

RESEARCH ARTICLE

NANO · MICRO small
www.small-journal.com

Catalytic Membrane Vacuum Regeneration: Enhancing Energy Efficiency and Renewable Compatibility in Direct Air Capture

*Arash Momeni, Rebecca V. McQuillan, Hossein Anisi, Masood S. Alivand, Ali Zavabeti, Geoffrey W. Stevens, Seungju Kim, and Kathryn A. Mumford**

Liquid-based CO_2 direct air capture (DAC) is a pivotal technology for mitigating climate change. Energy-intensive CO_2 desorption, high regeneration temperatures, and solvent degradation are key challenges. Here, low-temperature catalytic membrane vacuum regeneration (C-MVR) as a promising approach for sustainable and energy-efficient DAC is developed and evaluated. Noncatalytic experiments are conducted using three commercial membrane modules and four green amino acid salts under varying conditions (e.g., temperatures and flowrates). Based on CO_2 transfer rates, ultra-thin dense composite membranes and aqueous potassium taurinate (TauK) are the most promising for MVR in DAC applications. For C-MVR trials, commercial ion-exchange resin improves CO_2 desorption fluxes by up to 64.4% and reduces thermal energy requirements by up to 39.1%. TauK demonstrates the highest CO_2 flux and lowest thermal energy consumption. Parametric analysis of catalyst performance for varying temperatures, catalyst amount, and solvent concentrations is also performed. To minimize any potential precipitation in TauK, potassium carbonate (K_2CO_3) is added, showing minimal impact on CO_2 desorption kinetics and catalyst improvement. The findings of this study highlight the practical applicability of C-MVR using green amino acid salts as a sustainable approach to boost CO_2 desorption rate and reduce thermal energy input.

1. Introduction

Direct air capture (DAC) has emerged as a key climate solution by removing carbon dioxide directly from the atmosphere, offering a scalable way to reduce global emissions and support meeting the targets set by the Paris Agreement.[1–3] One of the major challenges in this field is the energy-intensive nature of the applied technologies (e.g., absorption and adsorption).[4] So far, considerable advancements have been made in adsorption systems using solid sorbents, enhancing energy efficiency and enabling the integration of sustainable heat sources.[5,6] This is while, for solvent-based approaches (despite their strong history of industrial application[7,8]) research and development have remained limited for DAC implementation. One of the key obstacles in this technology is the high energy demand of the solvent regeneration process, which typically requires boiling the solvent above 120 °C.[9,10] This not only hinders the use of sustainable energy sources but also poses a risk of thermal degradation of solvents.[11] The latter is particularly critical for amino acid salts, which are one of the most suitable solvents for DAC due to their favorable physicochemical properties, such as low volatility and toxicity and high oxidative stability.[12,13] In this regard, selecting and properly designing a contactor capable of low-temperature CO_2 desorption, along with implementing advanced, energy-efficient regeneration methods, is essential to making the liquid-based DAC process viable, cost-effective, and sustainable.

Membrane vacuum regeneration (MVR) using hollow fiber module contactors (HFMCs) is a reliable and well-established method for low-temperature CO_2 stripping.[14,15] The applied vacuum enables regeneration at 80–100 °C, reducing thermal energy demand and limiting solvent degradation over time.[16,17] Additionally, lower operating temperatures can be further coupled with renewable energy sources such as solar energy or low-grade heat, making DAC processes sustainable.[18] In this context, one of the most important factors in CO_2 transfer through membranes is the optimization of membrane characteristics and structure, which is crucial for minimizing mass

A. Momeni, R. V. McQuillan, H. Anisi, M. S. Alivand, A. Zavabeti, G. W. Stevens, K. A. Mumford
Department of Chemical Engineering
The University of Melbourne
Parkville, VIC 3010, Australia
E-mail: mumfordk@unimelb.edu.au
S. Kim
Department of Chemical and Environmental Engineering
School of Engineering
RMIT University
Melbourne, VIC 3000, Australia

The ORCID identification number(s) for the author(s) of this article can be found under https://doi.org/10.1002/smll.202503023

DOI: 10.1002/smll.202503023

Table 1. Specifications of three commercial HFMCs.

HFMCs	HFMC1	HFMC2	HFMC3
Membrane type and material	Porous PTFE	Dense PDMS	Ultra-thin PDMS composite
Module diameter [cm]	5.0	6.0	1.27
Module length [cm]	80	14	30
Effective fiber length [cm]	57.5	8.4	20
Number of fibers	240	12,600	160
Fiber ID [mm]	0.8	0.19	0.1
Fiber OD [mm]	1.57	0.3	0.374
PDMS wall thickness [µm]	-	55	0.9–1.2
Membrane area based on fiber OD [m^2]	0.68	1.0	0.0376

transfer resistance.[19] Hydrophobic porous membranes are commonly used for this purpose, however they are prone to pore wetting, which reduce performance.[20,21] This issue can be effectively addressed by using hydrophobic ultra-thin composite membranes, which a dense selective layer prevents liquid entering the pores.[22,23] Therefore, evaluating the performance of HFMCs with varying characteristics (especially ultra-thin composite membranes) is essential to further optimize and enhance the CO_2 transfer rates in low-temperature MVR under DAC conditions, which has not been experimentally studied yet.

Since DAC process is highly energy-intensive (ultra-low CO_2 partial pressure), integrating MVR with an additional low-temperature, energy-efficient technology would be highly beneficial.[24] Among different technologies,[25–27] catalytic solvent regeneration using heterogeneous solid acid-base catalysts is an emerging method that has shown promise in accelerating CO_2 stripping rates.[28] So far, a broad range of heterogeneous solid acid catalysts (e.g., zeolites, sulfated metal oxides, etc.) with various physicochemical properties have been developed and tested for this purpose under flue gas conditions,[29–31] with a few under DAC conditions.[32] However, to the best of the authors' knowledge, ion-exchange resins have not yet been investigated in liquid-based low-temperature CO_2 regeneration, either in flue gas specification or DAC, despite their promising characteristics and widespread use in various fields.[33–36] Availability, low cost, strong acidic functional groups, stability, macroporosity, and ease of operation are some of the important specifications of strong cation resins, making them a great candidate for evaluating its performance in catalytic solvent regeneration in MVR DAC.

Herein, we have developed and evaluated green energy-efficient catalytic membrane vacuum regeneration (C-MVR) for liquid-based DAC, which is an integrated system of catalytic solvent regeneration with vacuum membrane distillation operating in low temperature ranges (80–100 °C). Following from our previous studies in DAC systems,[32,37,38] we have developed a DAC desorption unit suitable for C-MVR tests. This work examines the performance of three HFMCs with various characteristics, including a polytetrafluoroethylene (PTFE) porous membrane, an ultra-thin polydimethylsiloxane (PDMS) dense layer composite membrane, and a non-porous PDMS membrane. The best-performing membrane with respect to its CO_2 separation efficiency and acceptable water transfer rate was selected and used to investigate the CO_2 desorption performance of four green amino acid salts (i.e., glycine, sarcosine, proline, and taurine) all with different and unique acidic and basic properties. Furthermore, the effect of process conditions (e.g., regeneration temperature) was studied. For C-MVR, a comprehensive set of trials of commercial acidic cation resins with different concentrations (3 and 6 wt%) for various solvents were conducted. To gain a better understanding of the catalyst performance under different conditions, the effects of regeneration temperature, solvent concentration, and additives were investigated. The findings of this study provide a strong foundation for applying a green, energy-efficient integrated system of catalytic solvent regeneration and MVR in sustainable DAC processes.

2. Experimental Section

2.1. Chemicals

Four types of amino acid salts with unique acidic and basic properties, namely glycine (Gly), sarcosine (Sar), and L-proline (Pro), all purity over 98% were purchased from Sigma–Aldrich. Taurine (Tau) was supplied by Consolidated Chemical Co., Australia (99.5% purity). Potassium hydroxide (KOH, >85.0% purity) was purchased from Chem-Supply, Australia. Solutions of potassium taurinate (TauK), potassium glycinate (GlyK), potassium sarcosinate (SarK), and potassium prolinate (ProK) were prepared by dissolving the respective amino acids in Milli-Q water with an equimolar quantity of KOH.

2.2. HFMCs

Three commercial membrane modules (Figure S1, Supporting Information) fabricated with different materials and structures were assessed and compared for their CO_2 transfer mechanisms (i.e., membrane distillation and pervaporation) and rates in DAC operation. **Table 1** shows the detailed specifications of the used HFMCs. Notably, for $HFMC_2$ and $HFMC_3$ the solvent was operated on the shell side whilst for $HFMC_1$ it was on the lumen side due to the large volume of the shell side.

2.3. Catalyst and Characterization

Ion-exchange resins are versatile, water-insoluble polymers with a cross-linked polystyrene backbone and ion-active side groups,

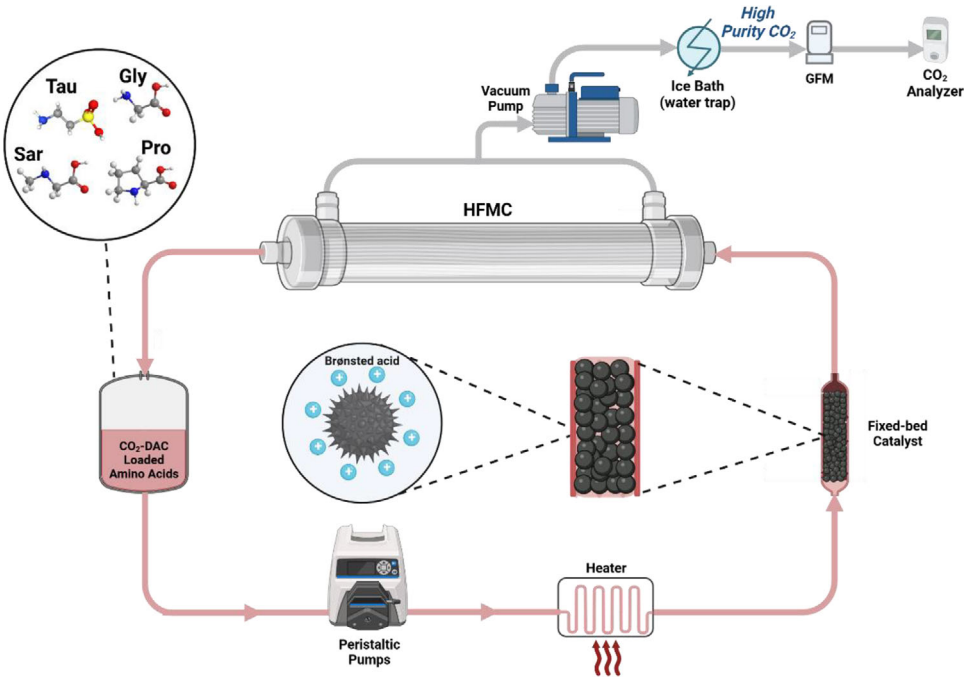

Figure 1. Scheme of the C-MVR apparatus for DAC.

that can be either positively or negatively charged. For this work, two types of strong acidic cation resins, Resin A and Resin B, composed of polystyrene crosslinked with divinylbenzene and containing negatively charged sites (sulfonic acid groups), were used for C-MVR trials. The structure, morphology, and elemental distribution of resins were fully characterized. Scanning Electron Microscopy (SEM) was conducted using the FEI Nova NanoSEM 200, an ultra-high-resolution (UHR) SEM equipped with a Field Emission Gun (FEG). UHR imaging was performed using the Through Lens Detector (TLD), with a spot size of 3.5 and an accelerating voltage below 10 kV. The instrument operated in immersion mode, utilizing the entire chamber as an objective lens to immerse the sample in a magnetic field for enhanced resolution. To prevent charging effects, samples were coated with a 1 nm iridium layer using the Leica EM ACE600 Sputter Coater prior to imaging. High-resolution transmission electron microscopy (TEM) was conducted with a JEOL JEM-F200 equipped with oxford EDX detector. X-ray photoelectron spectroscopy (XPS) experiments were done using Thermo Scientific K-alpha with Monochromated Aluminum Kα (1486.7 eV) source. Fourier Transform Infrared Spectroscopy (FTIR) ATR was collected using Bruker TESNOR II and CHNS was performed using Perkin Elmer 2400 Series II.

2.4. C-MVR Apparatus

For this study, the previously designed and developed MVR DAC rig[37] was used with further development. **Figure 1** shows the schematic view of the C-MVR apparatus (more details provided in Figure S2, Supporting Information). The loaded solvents under DAC condition using the procedure outlined in the previous work[32] (equilibrium values are reported in Figure S3, Supporting Information) was placed in the solvent reservoir. Using a peristaltic pump and an oil bath, the solvent was circulated (0.25 L.min^{-1}) and heated up to the desired set regeneration temperature, between 80 and 100 °C. At the solvent inlet and outlet of the HFMC, pressure gauges were installed to monitor the pressure drop during operation. One thermometer was used to record the temperature profile of the circulating solvent. Sample points were placed in the solvent loop to measure the CO_2 content of the solvent using the Chittick apparatus.[37] A vacuum pump was used to apply vacuum pressure on one side of the membrane (2–4 $kPa_{(a)}$), and a pressure gauge was used to monitor the vacuum pressure level. Two acetone-ice-baths were placed before the vacuum pump to condense and remove moisture from the high-purity CO_2 desorbed stream. The water collected at the end of each experiment was recycled back into the solvent container to ensure that the change in water content in the solvent remained minimal. To further analyze and accurately measure the high-purity CO_2 stream, a CO_2 analyzer and a flow meter were installed at the outlet of the vacuum pump. For C-MVR trials that include catalysts, a fixed bed was installed between the HFMC and oil batch heater so the solvent could get in contact with the catalyst after heating and before entering the HFMC.

2.5. Analysis of MVR Performance

To evaluate the performance of CO_2 desorption in MVR trials, Equation (1) was used:

$$J_{CO2} = \frac{N^{\circ} \times X_{co_2}}{A} \quad (1)$$

where J_{CO2} (mol.m^{-2}.s^{-1}) stands for CO_2 desorption flux, N° (mol.s^{-1}) and X_{CO2} are the molar flow and CO_2 concentration of

the outlet vacuum pump stream, respectively. A (m^2) is the effective surface area of the membrane.

To evaluate the water flux through the membrane, the rate of changing liquid level in the container was monitored during operation and compared to the water collected in acetone-ice-bath traps at the end of the experiment, which were in good agreement. Therefore, to calculate the water flux, Equation (2) was employed:

$$J_{water} = \frac{V}{A\Delta t} \quad (2)$$

where J_{water} ($mol.m^{-2}.s^{-1}$) is the water desorption flux, V (mol) is the collected water in the ice-bath trap, A (m^2) is the effective surface area of the membrane, and Δt (s) is the operational time frame.

For C-MVR tests, the CO_2 flux calculated using Equation (1). To assess the enhancement of the acidic cation resins, Equation (3) was used:

$$CE = \frac{J_{CO_2\_cat} - J_{CO_2}}{J_{CO_2}} \times 100 \quad (3)$$

where CE (%) is the catalyst enhancement of the system, $J_{CO2\text{-}cat}$ and J_{CO2} ($mol.m^{-2}.s^{-1}$) are the CO_2 desorption flux with and without solid acid catalysts.

The thermal energy consumption ($GJ.tCO_2^{-1}$) of the solvent in HFMC was evaluated using Equation (4):

$$Q = \eta \left(mc_p\Delta T\right) / \left(J_{CO_2} M_w A\Delta t\right) \quad (4)$$

where m (kg) is the total mass of solvent in the system, cp ($kJ.kg^{-1}.°C^{-1}$), and ΔT (°C) are the mass heat capacity and solvent temperature change, respectively, J_{CO2} ($mol.m^{-2}.s^{-1}$)is the recorded CO_2 flux, M_w ($g.mol^{-1}$) is the CO_2 molecular weight, A (m^2) and Δt (s) are membrane surface area and operation time. It is important to note 90% heat recovery, considering an efficient rich/lean heat exchanger was assumed (η to be equal to 0.1). Additionally, for the calculated thermal energy consumption, an average operation time of 90 min was considered.

The relative heat duty (%) was calculated according to Equation (5):

$$RH = \frac{Q_{Cat}}{Q_{Blank}} \times 100 \quad (5)$$

where Q_{Cat} and Q_{Blank} are the thermal energy consumption ($GJ.tCO_2^{-1}$) with and without catalyst, respectively.

3. Results and Discussion

3.1. Membrane Module Performance

Initially, three different HFMCs, each with distinct characteristics, membrane resistance, and CO_2 transfer mechanism, were considered and evaluated (Table 1; Figure S1, Supporting Information). These tests were conducted using 3 M GlyK at 90 °C. In selecting a suitable membrane module for liquid-based DAC operations, CO_2 flux plays a critical role, while the water transfer rate through the fibers is also an important consideration. The latter significantly impacts the size and energy requirements for the condenser and vacuum pump, as well as the ease of MVR operation on a large scale. As illustrated in **Figure 2a–c**, $HFMC_3$ exhibited the highest CO_2 flux and the lowest water to CO_2 flux ratio in the MVR DAC. This is primarily related to the coated ultra-thin PDMS layer (a rate-determining layer for CO_2 permeance), which minimizes membrane resistance and accelerates CO_2 transfer. Furthermore, due to the pervaporation mechanism governing the transfer process, CO_2 selectivity was enhanced.[39,40] Interestingly, despite having a porous structure and the lowest membrane resistance of $HFMC_1$, It showed lower CO_2 flux as compared to $HFMC_3$. A primary cause for this behavior is pore wetting, a common issue in porous membrane modules that leads to reduced CO_2 removal efficiency. This issue can be minimized by adjusting the membrane pore size and hydrophobicity (material selection).[41] The significant water flux, due to water convective flow through the larger pores, and consequently high ratio of water to CO_2 flux indicates the occurrence of this issue in $HFMC_1$. Among the HFMCs, $HFMC_2$ demonstrated both the lowest CO_2 and water flux. This is mainly related to the existence of a thick hydrophobic dense PDMS layer (55 µm), which considerably increases membrane resistance and lowers both CO_2 and water flux. Despite having the lowest water flux, the CO_2 flux for $HFMC_2$ is 58.3% lower than $HFMC_3$, highlighting the rate-determining effect of the PDMS layer thickness. Hence, $HFMC_3$ (the ultra-thin dense membrane layer) was selected as the suitable membrane for further MVR DAC analysis. Top-view and cross-sectional SEM images, along with EDX elemental analysis of the $HFMC_3$ fibers, are provided in Figure S4 (Supporting Information). To measure the accuracy and repeatability of the rig and the experiments, two more trials were conducted at 90 °C with $HFMC_3$ using 3 M GlyK. The results are shown in Figure S5 (Supporting Information), highlighting compelling accuracy and repeatability of the MVR apparatus.

3.2. Amino Acids Performance

Figure 2d,e illustrates the performance of four amino acid salts, including TauK, GlyK, SarK, and ProK with a concentration of 3 M in the MVR DAC system. Due to the thermal stability of $HFMC_3$, 100 °C was selected as the operating temperature. Figure 2d shows the CO_2 flux profiles of the amino acid salts along with their temperature profiles over time. As the solvent temperature increased and approached 90–100 °C, the CO_2 analyzer and flow meter started detecting high purity CO_2 at the vacuum pump outlet. The observed delay between the temperature profile and CO_2 detection is due to the low amount of desorbed CO_2 (because of the low surface area of $HFMC_3$) and the volume of the system before the CO_2 analyzer. As the operation continued at the stabilized temperature, the CO_2 flux increased and achieved the stabilized conditions, which was considered the final CO_2 flux for the trial. Comparing the stabilized flux reported in Figure 2e, TauK demonstrated the highest CO_2 transfer rate, being 59.4% greater than GlyK. This can primarily be attributed to the sulfonic acid group ($SO_3^-H^+$), which gives taurine acidic properties, making it easier to deprotonate during regeneration and release protons. This facilitates the breakdown of carbamate, liberating greater

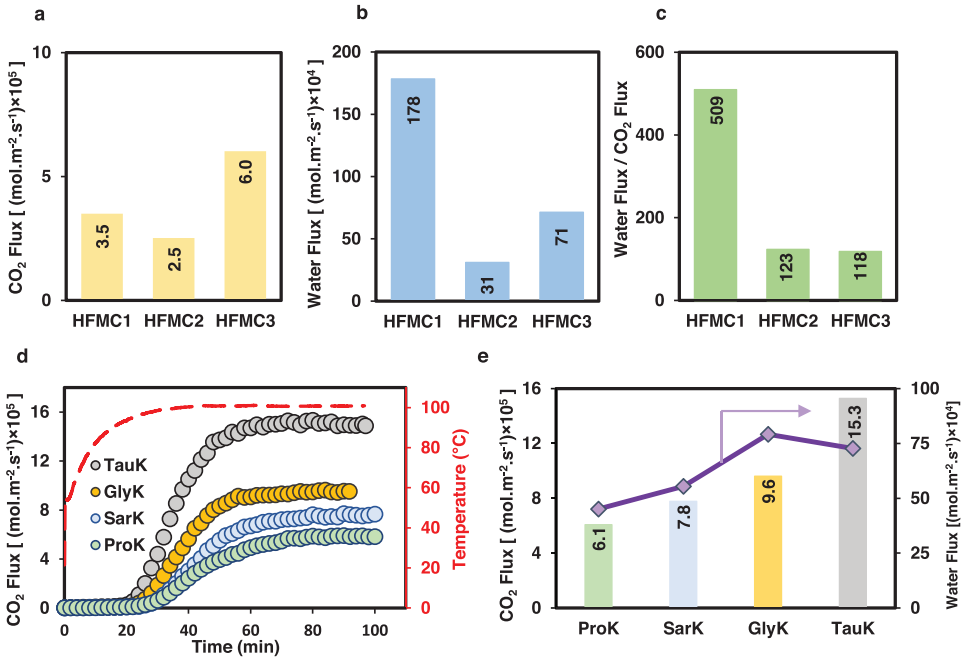

Figure 2. a) CO_2 flux, b) water flux, and c) ratio of water to CO_2 flux for three used HFMCs at 90 °C. d) CO_2 desorption profiles over time, and e) water flux and CO_2 flux of various 3 M amino acids at 100 °C. All trials were accomplished at 2–4 kPa(a), 0.25 $L.min^{-1}$.

amounts of CO_2 from the solution which is consistent with our observation in recent study.[42] For the other solvents, GlyK, SarK, and ProK were in descending order of the CO_2 flux, respectively. These results are well aligned with our previous study on the DAC cyclic capacity of various solvents in the temperature range of 25–98 °C.[32] For determining the water transfer rate for different solvents in $HFMC_3$, the amount of water collected in each trial was accurately measured. Figure 2e shows that GlyK exhibited the highest water flux, followed by TauK and SarK in second and third place, respectively, while ProK recorded the lowest. The order and behavior can be likely attributed to the hydrophobicity and hydrophilicity degree of the amino acid salts. It is notable that the high CO_2 flux for TauK resulted in the lowest water to CO_2 ratio flux among the examined solvents. This, combined with the remarkable thermal stability of TauK,[42] makes it a suitable choice for MVR DAC.

3.3. Solvent Temperature and Flow Rate

To gain a better understanding of the MVR DAC process, the role of crucial parameters such as regeneration temperature and solvent flow rate were assessed on the CO_2 flux. Two amino acid salts, 3 M TauK and 3 M GlyK (**Figure 3a**), having the highest CO_2 desorption kinetics among the studied solvent were selected to screen their performance in temperature ranges of 80–100 °C. Figure 3b depicts the various temperature profiles and corresponding CO_2 desorption curves for 3 M TauK over time. As illustrated, an increase in temperature leads to an increase in CO_2 desorption kinetics, driven by a higher CO_2 equilibrium partial pressure, and reaction rate across the membrane. Notably, the trials using lower temperatures were longer due to the reduced number of desorbed CO_2 moles and, consequently, more time was needed to achieve a stabilized condition. Figure 3c shows the stabilized CO_2 flux values for 3 M TauK and 3 M GlyK, where in all temperature ranges, TauK outperforms GlyK. Additionally, TauK significantly enhanced its CO_2 desorption performance (over ≈180%, from 5.4×10^{-5} to 15.3×10^{-5} $mol.m^{-2}.s^{-1}$) by increasing the temperature from 80 to 100 °C, while GlyK showed ≈120% improvement (4.3×10^{-5}–9.6×10^{-5} $mol.m^{-2}.s^{-1}$). This is mainly attributed to the different molecular structures of the two amino acids and the presence of a sulfonic acid group in TauK, which is more effective for proton exchange (TauK deprotonation) at high temperatures.[29,32] Hence, to maximize the CO_2 desorption efficiency of the MVR in DAC, 100 °C was chosen as a suitable regeneration temperature.

The hydrodynamics of the MVR system are another key feature that was evaluated. Figure 3d highlights the effect of solvent flow rate on CO_2 desorption performance for 3 M GlyK at 100 °C. As shown, a minor change was observed as the flow rate decreased from 0.25 to 0.05 $L.min^{-1}$. The Reynolds number (Re) (Figure 3d) in these flow ranges suggested that the solvent flow stayed in the laminar regime. This can explain the non-effectiveness of the solvent flow rate on the stripping performance. Thus, more experiments can be accomplished in the future in a wider range of solvent flow rates and Re values to analyze the hydrodynamic effects on the performance of the system in DAC. Additionally, it would be advantageous for MVR to operate at a lower solvent flow rate with a specific and constant efficiency, as this would require less thermal energy for continuous solvent heating.

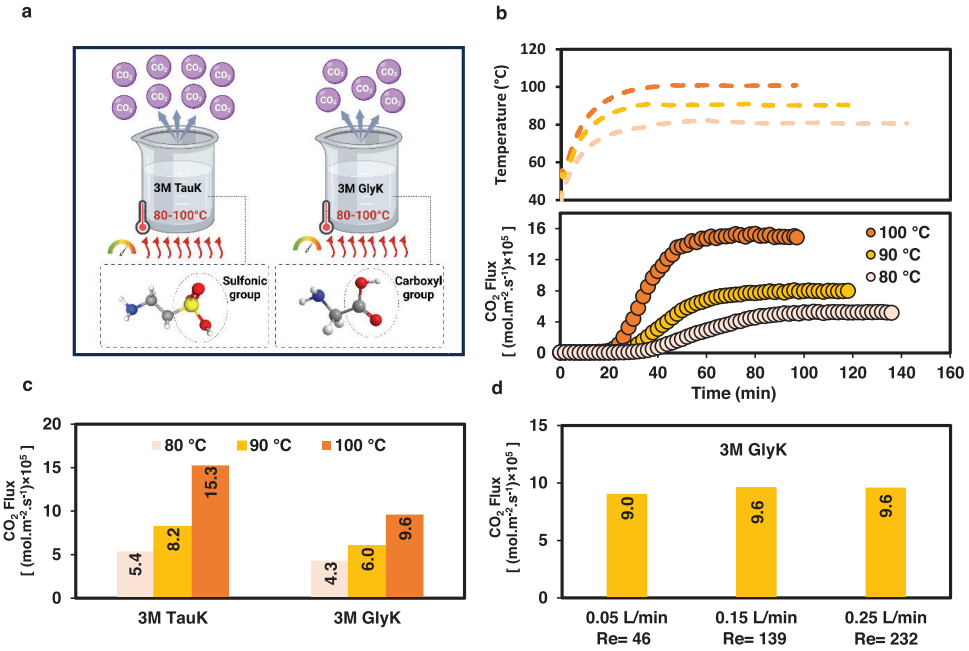

Figure 3. a)cb) 3 M TauK CO_2 desorption profiles over time at various temperatures. c) 3 M TauK and GlyK CO_2 flux at various temperatures. d) 3 M GlyK CO_2 flux at 100 °C under different solvent flow rates. All trials were accomplished at 2–4 $kPa_{(a)}$. Solvent flow rates set to 0.25 $L.min^{-1}$ for (b,c).

3.4. Catalytic Membrane Vacuum Regeneration (C-MVR)

For C-MVR DAC trials, a catalyst fixed bed filled with strong, acidic resin beads functionalized with $SO_3^-H^+$ (schematically shown in **Figure** 4a) was added to the solvent circulation loop to analyze its effect on CO_2 desorption kinetics. Two types of ion exchange resins were employed with distinct physicochemical properties, crosslinking, and acidic strength.

To start the C-MVR DAC trials, a concentration of 3wt% was selected for both types of catalysts (Resin A and B) to analyze their impact on enhancing CO_2 desorption kinetics. Based on our previous study,[32] since GlyK showed considerable desorption improvement with acidic catalysts, the first catalytic trials assessed 3 M GlyK being regenerated at 100 °C. Interestingly, Resin B, resulted in negligible improvement in the CO_2 desorptive flux. However, Resin A exhibited an enhancement in CO_2 flux by 21.2%. Based on the SEM and TEM results (Figure 4a; Figures S6, S7, Supporting Information), both catalysts showed the same morphology, porous amorphous structure, and bead size distributions. TEM-EDX mapping on crushed catalysts further confirmed the integrated distribution of carbon, sulfur, and oxygen (Figure 4a; Figure S6e, Supporting Information). However, XPS results highlighted that Resin A had threefold more sulfur content (14.8 at.%) compared to Resin B (4.8%), a strong indicator of an increased amount of Brønsted acid sites (Figure 4b). Brønsted acid sites play a crucial role in enhancing catalyst performance by effectively acting as proton donors. This functionality facilitates key reactions such as deprotonation and carbamate breakdown, thereby improving CO_2 desorption rates.[28] Several studies in the literature have discussed possible catalytic mechanisms, most of which focus on 5 M monoethanolamine (MEA) solvent under flue gas conditions.[30] A few works have investigated amino acid solvents,[27,43] particularly in the context of DAC.[32] Nevertheless, nearly all studies follow a similar mechanistic pathway involving three main steps: 1) chemisorption and proton transfer, 2) structural rearrangement (isomerization), and 3) dissociation.

To further investigate the properties of the resins, Figure 4c,d depicts the XPS analysis for S2p spectrum of the two catalysts, Resin A and B, respectively. The binding energies at 168.5 (i.e., S 2p3/2) and 169.7 eV (i.e., S2p1/2), related to SOH and SO, confirm the presence of $-SO_3^-H^+$ groups.[27,44] Comparing the intensity peaks in the XPS spectra of Figure 4c,d, Resin A intensity peaks are considerably higher than Resin B, highlighting stronger acidity. Further analysis by XPS characterization was performed for O1s, and C1s of Resin A (Figure S8a,b, Supporting Information) to also show carbon, O—H and O—S binding energies. Additionally, characterization using FTIR (Figure S9, Supporting Information) confirmed the XPS results (Figure 4b–d). To accurately measure the elemental content of the catalysts, CHNS analysis was conducted and reported in Table S1 (Supporting Information). Based on the reported values, the normalized sulfur to carbon ratio (S/C) for Resin A is four times higher than for Resin B, which confirms a stronger acidity. Therefore, for the rest of the C-MVR experiments, Resin A was utilized.

Figure 4e shows the CO_2 desorption performance of 3 M TauK with (3 and 6 wt%) and without catalyst (blank). Comparing the curves with the blank, it is compelling to see that the CO_2 flux ramp starts at lower temperature ranges when the catalyst is present. This highlights the impact of the resin beads on the MVR process, which can facilitate and increase the quantity of CO_2 liberated by exchanging protons in lower temperature ranges in a certain timeframe. This results in an increase in the CO_2 partial pressure on the liquid side of the membrane module, ultimately leading to a higher CO_2 flux. Continuing the

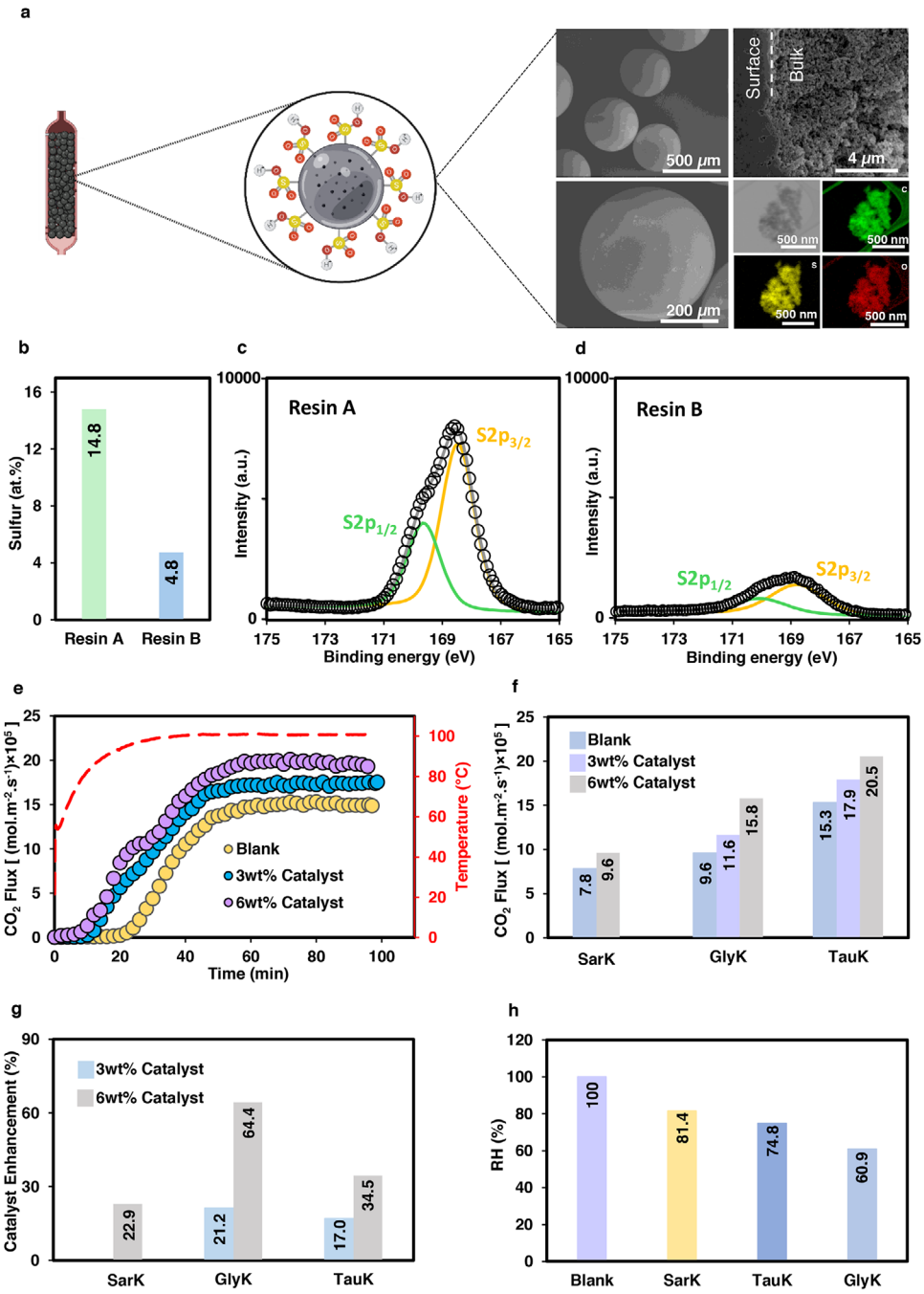

Figure 4. a) Schematic diagram of acidic cation resins, SEM images and TEM-EDX mapping of Resin A. b) Sulfur content analyzed by XPS for two cation resins. c) High-resolution XPS spectra of Resin A, and d) Resin B. e) 3 M TauK CO_2 desorption profiles over time, and f) CO_2 flux values for various 3 M amino acids without/with catalyst for different concentrations. g) Catalyst enhancement values for different concentrations and various 3 M amino acids. h) Relative heat duty using 6wt% catalyst for 3 M amino acids. All trials were accomplished at 100 °C, 2–4 $kPa_{(a)}$, 0.25 $L.min^{-1}$, using Resin A. No catalyst was used for blank solvent.

operation at a constant regeneration temperature, the CO_2 flux curves stabilized at 15.3×10^{-5}, 17.9×10^{-5}, and 20.5×10^{-5} $mol.m^{-2}.s^{-1}$ for the blank, 3 and 6 wt% catalyst, respectively, equivalent to a 17.0% and 34.5% enhancement (Figure 4f,g). The result shows that by doubling the catalyst concentration for TauK, the enhancement is also doubled. In addition, it demonstrates the effectiveness and applicability of acidic cation resins in a fixed bed in the MVR process using an ultra-thin dense layer membrane.

To evaluate the catalyst impact on different amino acid salts with different molecular structures and CO_2-containig species, the same trials were conducted for 3 M GlyK and SarK. According to Figure 4f,g, in the presence of 3 and 6 wt% resin beads, the

Table 2. Thermal energy consumption for well-established DAC technologies.

Technology	System type	Thermal energy needs	Thermal energy consumption ($GJ.tCO_2^{-1}$)	Thermal energy source	Refs.
Carbon Engineering	Liquid solvent	900 °C	5.3–8.81	Natural gas with CCS	[46,47]
Climeworks	Solid sorbent	80–120 °C	5.8–14.5	Non-fossil energy resources (geothermal, waste heat)	[6,48,49]
Global Thermostat Company	Solid sorbent	105–120 °C	4.4	Energy resource agnostic	[47,49]

GlyK CO_2 desorption performance was promoted by 21.2% and 64.4%, respectively, with the latter being the highest observed catalyst improvement. Interestingly, for SarK, which has the highest DAC-loaded saturation point (420 ppm CO_2 and 25 °C) compared to TauK and GlyK (Figure S3, Supporting Information) demonstrated the poorest catalytic effect, only 22.9% in the presence of a 6wt% catalyst. As reported in our previous study on catalytic solvent regeneration in the DAC process,[32] the acidic catalyst had the highest impact on CO_2 desorption with GlyK and the least impact with SarK among the short-chain amino acids. Several factors may contribute to this behavior, including the nature of CO_2-containing species, the strength of acidity and basicity (pKa values), molecular weight, and water solubility.[27] To gain a better understanding of how these parameters influence catalytic performance, a comprehensive study involving various amino acids with different physicochemical properties should be conducted in future work. In the case of TauK, despite its large cyclic CO_2 capacity,[42] it exhibited a lower catalytic effect compared to GlyK. One possible reason is the presence of a sulfonic acid group in the taurine structure, which facilitates the deprotonation of protonated taurine and increases the availability of free protons. This could reduce the relative impact of the catalyst when compared to GlyK.

Figure 4h shows the relative heat duty using a 6wt% catalyst for different solvents. Considering the catalyst performance, GlyK and TauK exhibited a 39.1%, and 25.2% reduction in thermal energy input, respectively. Nonetheless, among all the conducted C-MVR trials, the highest recorded CO_2 flux was for TauK (20.5 × 10^{-5} $mol.m^{-2}.s^{-1}$) which was 29.7% more than GlyK (15.8 × 10^{-5} $mol.m^{-2}.s^{-1}$) (Figure 4f). CO_2 flux is a critical parameter in the MVR process, as it influences overall efficiency, solvent cyclic capacity, system size, and both capital and operating costs. To further investigate, the CO_2 transfer rates for the 6 wt% catalyst were used to estimate the thermal energy consumption in the C-MVR system using Equation (4). The results showed thermal energy consumption of 8.6 $GJ.tCO_2^{-1}$ for TauK and 11.2 $GJ.tCO_2^{-1}$ for GlyK. Despite TauK's lower catalyst enhancement and higher relative heat duty, its higher CO_2 flux led to a 23.2% reduction in final energy consumption compared to GlyK.

To compare the regeneration energy of the current system with other DAC technologies, the total thermal energy consumption was estimated by adding the enthalpy of desorption for 3 M TauK (2.04 $GJ.tCO_2^{-1}$)[45] to the calculated energy input (8.6 $GJ.tCO_2^{-1}$), resulting in a total of 10.6 $GJ.tCO_2^{-1}$. **Table 2** summarizes the reported thermal energy requirements of several well-established DAC technologies.

Due to various reported energy consumption for number of technologies in Table 2, a range of values is provided. While Carbon Engineering's liquid-based DAC process demonstrates relatively lower energy consumption, it operates at extremely high temperatures (≈900 °C), which require heat from fossil fuel combustion. Compared to other DAC systems in Table 2, a particularly promising and green sustainable approach is the temperature-vacuum swing adsorption (TVSA) process, which employs amine-functionalized, biodegradable cellulose sorbents. This system captures CO_2 and regenerates it under vacuum at temperatures between 80 and 120 °C.[6] Notably, TVSA is also the core technology used by Climeworks. Comparing the energy consumption of the TVSA process with the C-MVR system developed in this work, the values fall well within the same range. This highlights the potential of the C-MVR system as sustainable and scalable liquid-based DAC technology.

Notably, using a larger ultra-thin dense membrane module with greater surface area than $HFMC_3$ could enhance the total number of CO_2 desorption and further reduce energy consumption which is a part of future work of this study.

3.5. Catalyst Impact by Solvent Condition

To further examine crucial variables in the C-MVR process, the catalyst effectiveness was investigated at lower temperature ranges (90 °C) for TauK and GlyK with the highest observed catalytic effect on CO_2 desorption performance. All trials were accomplished with a fixed catalyst concentration of 6 wt%. The CO_2 desorption curves at 90 °C are depicted in **Figure 5**a,b, and the corresponding final stabilized CO_2 flux and catalyst improvements are shown in Figure 5f. Comparing the results with 100 °C (Figure 4f,g), it can be seen that by decreasing the regeneration temperature, the ultimate CO_2 flux and the catalytic impact both decrease. In fact, a 10 °C decrease in regeneration temperature reduced the catalyst performance from 64.4% to 48.9% for 3 M GlyK and from 34.5% to 20.7% for 3 M TauK. Notably, the CO_2 flux for TauK was halved. Hence, increasing the temperature enhanced catalyst activation in the process.[32]

One of the limitations of applying green amino acids on a large scale is the potential formation of solids in the solution in lower absorption temperature ranges, and at high CO_2 loadings or high solvent concentrations.[17] This can cause operational problems and reduce the CO_2 uptake rate.[50] It is notable that during CO_2 absorption in the TauK (near its saturation point) and after C-MVR trials, the formation of solids was noticed in the solution. Therefore, considering the ultra-low partial pressure of CO_2 in air, which contributes to lower saturation points in DAC processes, the CO_2 desorption performance was assessed at two additional TauK concentrations (2 M and 2.5 M). The evaluations were conducted both with and without catalysts to assess system efficiency and monitor any potential precipitation. The results

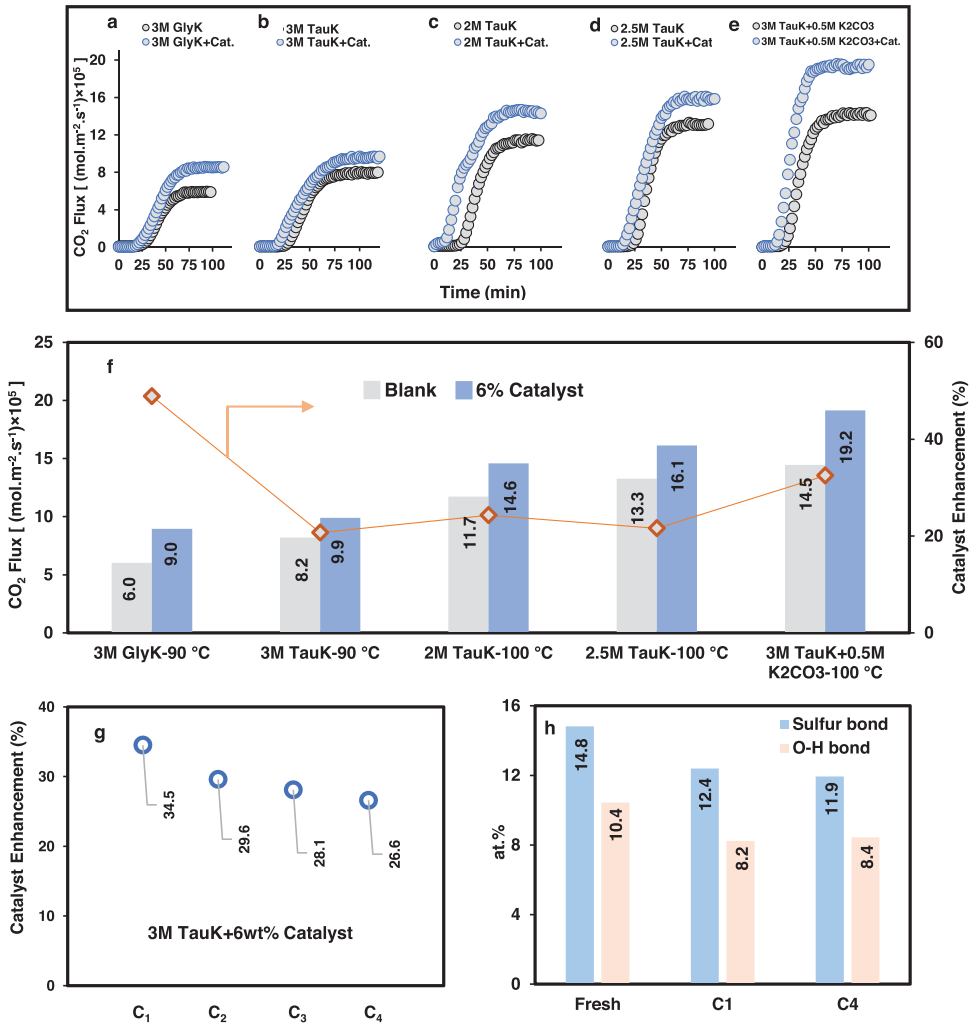

Figure 5. a) CO_2 desorption profiles for GlyK, and b) TauK with/without catalyst at 90 °C. c) CO_2 desorption profiles for 2 M TauK, d) 2.5 M TauK, and e) 3 M TauK+0.5 M K_2CO_3 with/without catalyst at 100 °C. f) CO_2 flux and catalyst enhancement values for (a-e). g) Catalyst stability in four cycles. h) Sulfur and O—H bond content for fresh, first and forth cycles. All trials were accomplished at 2–4 kPa (a), 0.25 L.min^{-1}, using Resin A (6 wt% concentration).

revealed that lowering the solvent concentration significantly minimized precipitation (Figure S10, Supporting Information). However, as expected, Figure 5c,d,f shows that reducing the TauK concentration from 3 M to 2.5 M and 2 M led to a decline in both CO_2 flux and catalyst effectiveness. In fact, in the presence of 6 wt% catalyst, comparing the CO_2 transfer rate of 3 M to 2 M TauK at 100 °C, a 28.8% loss (20.5×10^{-5}–14.6×10^{-5} mol.m^{-2}.s^{-1}) was observed. The reduction can be ascribed to a decrease in the number of solvent molecules in the solution, causing a decrease in the number of carbamate molecules. This can negatively affect the proton exchange mechanism of catalysts and subsequent CO_2 flux across the membrane. Therefore, to keep the CO_2 flux and efficiency of the C-MVR as high as possible without any potential precipitation in the process, potassium carbonate (K_2CO_3) was used as an additive to 3 M TauK solution and tested in the C-MVR rig at 100 °C. K_2CO_3 is widely recognized as a suitable solvent for CO_2 removal in a range of industries due to its stability, environmental friendliness, and cost-effectiveness.[51] However, its slow reaction rate with CO_2 poses significant challenges for its widespread application.[52,53] In this study, K_2CO_3 was selected as a 0.5 M additive to the 3 M TauK solution due to its buffering effect, which helps control pH and minimize precipitation.[54–56] Figure 5e,f shows the resulting CO_2 desorption performance curves, CO_2 fluxes, and catalyst enhancement for the 3 M TauK+0.5 M K_2CO_3 solution. Compared to the results of 3 M TauK, the formation of precipitation in the solvent used was significantly reduced (Figure S10, Supporting Information). The CO_2 transfer rate and catalyst effect showed only a minimal reduction, from 34.5% (Figure 4f,g) to 32.5% (Figure 5e,f), despite the basic behavior of the added K_2CO_3, which could adversely affect the regeneration process. Considering these observations, optimizing the concentrations of TauK and K_2CO_3 would be beneficial to further adjust the CO_2 transfer rate, minimize any potential precipitation, and operational issues.

3.6. Catalyst Stability

The stability of ion exchange resins was investigated in the four consecutives C-MVR trials at 100 °C for 3 M TauK. As shown in Figure 5g, the catalyst performance dropped by 4.9% for the first cycle followed by 1.5% reduction for the second and third. The latter reduction highlighted the successful and continuous proton exchange mechanism in the catalytic solvent regeneration process for resin beads which can recover the lost protons. Furthermore, XPS analysis confirmed the stability in intensity of SOH and SO groups and content of sulfur and O—H bonds in different cycles of the catalyst (Figure 5h; Figure S8c, Supporting Information). Also, it is notable that for full recovery of acidic cation resins after long-term operation, it can easily be regenerated by strong acids such as sulfuric acid (H_2SO_4) or hydrochloric acid (HCl).

4. Conclusion

To summarize, in this study, a sustainable integrated system of solid acid catalysts (ion exchange resins) and low-temperature membrane vacuum regeneration (MVR) using green amino acid salts was developed and analyzed for use in DAC systems. For non-catalytic trials, various commercial membrane modules with distinct features and transfer mechanisms (membrane distillation and pervaporation) were assessed. Ultra-thin dense PDMS composite membrane was selected as a suitable contactor for MVR in DAC. Among the four screened green amino acid salts, TauK exhibited the highest CO_2 separation performance (59.4% higher compared to GlyK). Further parametric analysis was performed at different regeneration temperatures (80–100 °C) and solvent flow rates (0.05–0.25 L.min^{-1}). From 80 to 100 °C, a major improvement (over ≈180%) in CO_2 desorption performance was measured for TauK and no considerable effect was observed by a change in solvent flow. For catalytic experiments (C-MVR), the performance of 3 and 6 wt% of commercial acidic cation resins with various green amino acid salts was assessed. The results showed that doubling the catalyst concentration doubles or triples the catalyst effectiveness, depending on the solvent type. Among the amino acid salts, the maximum catalyst enhancement (using 6wt% concentration) was observed on GlyK with a value of 64.4%, followed by 34.5% for TauK. The catalyst enhancement resulted in up to a 39.1% reduction in thermal energy input. Despite the lower catalytic impact on TauK, the highest CO_2 flux and lowest thermal energy consumption values were recorded for TauK. Furthermore, a 10 °C decrease in regeneration temperature resulted in a ≈14–15% reduction in the catalyst enhancement parameter (CE%). To minimize any potential solid formation in TauK, C-MVR trials at lower concentrations and in the presence of K_2CO_3 as an additive were conducted. Lower solvent concentrations resulted in lower CO_2 desorption rates and catalyst effects. Additionally, adding K_2CO_3 minimized solid formation and had a minimal effect on the CO_2 desorption performance and catalyst effect. The results of this study clearly illustrate the suitability of integrating catalyst solvent regeneration with MVR for a sustainable and energy-efficient liquid-based DAC.

Supporting Information

Supporting Information is available from the Wiley Online Library or from the author.

Acknowledgements

Open access publishing facilitated by The University of Melbourne, as part of the Wiley - The University of Melbourne agreement via the Council of Australian University Librarians.

Conflict of Interest

The authors declare no conflict of interest.

Data Availability Statement

The data that support the findings of this study are available from the corresponding author upon reasonable request.

Keywords

amino acids, catalytic solvent regeneration, direct air capture, hollow fiber membranes, low-temperature regeneration

Received: March 7, 2025
Revised: April 10, 2025
Published online: April 27, 2025

[1] A. Kasturi, G. G. Jang, A. Dona-Tella Akin, A. Jackson, J. Jun, D. Stamberga, R. Custelcean, D. S. Sholl, S. Yiacoumi, C. Tsouris, *Separation Purif. Technol.* **2023**, *324*, 124398.
[2] M. Ozkan, S. P. Nayak, A. D. Ruiz, W. Jiang, *iScience* **2022**, *25*, 103990.
[3] C. A. Seipp, N. J. Williams, M. K. Kidder, R. Custelcean, *Angew. Chem. Int. Ed. Engl.* **2017**, *56*, 1042.
[4] A. Sodiq, Y. Abdullatif, B. Aissa, A. Ostovar, N. Nassar, M. El-Naas, A. Amhamed, *Environ. Technol. Innov.* **2023**, *29*, 102991.
[5] X. Zhu, W. Xie, J. Wu, Y. Miao, C. Xiang, C. Chen, B. Ge, Z. Gan, F. Yang, M. Zhang, D. O'Hare, J. Li, T. Ge, R. Wang, *Chem. Soc. Rev.* **2022**, *51*, 6574.
[6] H. Akaya, S. Lamnini, H. Sehaqui, J. Jacquemin, *ACS Appl. Mater. Interfaces* **2025**, *17*, 16380.
[7] S. Wang, C. Shang, Y. Deng, J. Baeyens, T. V. Plisko, A. V. Bildyukevich, T. M. Aminabhavi, X. Liu, M. Moyo, H. Liu, *Chem. Eng. J.* **2024**, *480*, 147918.
[8] G. Li, X. Shen, X. Jiao, F. Xie, J. Hua, H. Lin, F. Yan, H. Wu, Z. Zhang, *Chem. Eng. J.* **2024**, *493*, 152699.
[9] F. Sabatino, A. Grimm, F. Gallucci, M. van Sint Annaland, G. J. Kramer, M. Gazzani, *Joule* **2021**, *5*, 2047.
[10] K. An, K. Li, C.-M. Yang, J. Brechtl, K. Nawaz, *J. CO2 Util.* **2023**, *76*, 102587.
[11] T. Supap, S. Chintana, I. Raphael, P. P. T. Tontiwachwuthikul, *Carbon Manage.* **2011**, *2*, 551.
[12] F. M. Brethomé, N. J. Williams, C. A. Seipp, M. K. Kidder, R. Custelcean, *Nat. Energy* **2018**, *3*, 553.
[13] K. An, K. Li, C.-M. Yang, J. Brechtl, D. Stamberga, M. Zhang, K. Nawaz, *AIChE J. n/a (n/a)*, 18429.
[14] J. M. Vadillo, G. Díaz-Sainz, L. Gómez-Coma, A. Garea, A. Irabien, *Membranes* **2022**, *12*, 785.

[15] C. A. Scholes, *Chem. Eng. Sci.* **2023**, *278*, 118915.
[16] Z. Zhang, Y. Li, W. Zhang, J. Wang, M. R. Soltanian, A. G. Olabi, *Renewable Sustainable Energy Rev.* **2018**, *98*, 179.
[17] R. Ramezani, S. Mazinani, R. Di Felice, *Rev. Chem. Eng.* **2022**, *38*, 273.
[18] M. S. Alivand, G. W. Stevens, K. A. Mumford, *Nat. Commun.* **2023**, *14*, 4137.
[19] S. Kim, C. A. Scholes, D. E. Heath, S. E. Kentish, *Chem. Eng. J.* **2021**, *411*, 128468.
[20] M. H. Ibrahim, M. H. El-Naas, Z. Zhang, B. Van der Bruggen, *Energy Fuels* **2018**, *32*, 963.
[21] K. Xue, H. Fu, H. Chen, H. Zhang, D. Gao, *Sep. Purif. Technol.* **2023**, *304*, 122309.
[22] C. A. Scholes, S. E. Kentish, G. W. Stevens, J. Jin, D. deMontigny, *Sep. Purif. Technol.* **2015**, *156*, 841.
[23] Z. Dai, L. Ansaloni, L. Deng, *Ind. Eng. Chem. Res.* **2016**, *55*, 5983.
[24] X. Wang, C. Song, *Front. Energy Res.* **2020**, *8*, 560849.
[25] M. S. Alivand, O. Mazaheri, Y. Wu, G. W. Stevens, C. A. Scholes, K. A. Mumford, *Appl. Energy* **2019**, *256*, 113911.
[26] F. Liu, M. Fang, W. Dong, T. Wang, Z. Xia, Q. Wang, Z. Luo, *Appl. Energy* **2019**, *233*, 468.
[27] M. S. Alivand, O. Mazaheri, Y. Wu, A. Zavabeti, G. W. Stevens, C. A. Scholes, K. A. Mumford, *ACS Appl. Mater. Interfaces* **2021**, *13*, 57294.
[28] M. S. Alivand, O. Mazaheri, Y. Wu, A. Zavabeti, A. J. Christofferson, N. Meftahi, S. P. Russo, G. W. Stevens, C. A. Scholes, K. A. Mumford, *Nat. Commun.* **2022**, *13*, 1249.
[29] M. S. Alivand, O. Mazaheri, Y. Wu, G. W. Stevens, C. A. Scholes, K. A. Mumford, *ACS Sustainable Chem. Eng.* **2020**, *8*, 18755.
[30] T. Li, Q. Yu, F. Barzagli, C. E. Li, M. Che, Z. Zhang, R. Zhang, *Carbon Capture Sci. Technol.* **2023**, *6*, 100099.
[31] X. Zhang, Z. Zhu, X. Sun, J. Yang, H. Gao, Y. Huang, X. Luo, Z. Liang, P. Tontiwachwuthikul, *Environ. Sci. Technol.* **2019**, *53*, 6094.
[32] M. S. Alivand, R. V. McQuillan, A. Momeni, A. Zavabeti, G. W. Stevens, K. A. Mumford, *Small* **2023**, *19*, 2300150.
[33] J. Hegarty, B. Shindel, D. Sukhareva, M. L. Barsoum, O. K. Farha, V. Dravid, *Environ. Sci. Technol.* **2023**, *57*, 21080
[34] W. A. El-Mehalmey, A. H. Ibrahim, A. F. A. Youssef, O. Abuzalat, M. S. Mousa, A. S. Mayhoub, M. H. Alkordi, *ACS Appl. Mater. Interfaces* **2023**, *17*, 17684.
[35] T. Vu, T. T., S. Liu, M. Jonušis, S. Jonušienė, J. Choi, R. Kawano, N. Rehnberg, R. Hatti-Kaul, S.-H. Pyo, *ACS Sustainable Chem. Eng.* **2023**, *11*, 17130.
[36] Q. Shu, M. Haug, M. Tedesco, P. Kuntke, H. V. M. Hamelers, *Environ. Sci. Technol.* **2022**, *56*, 11559.
[37] A. Momeni, R. V. McQuillan, M. S. Alivand, A. Zavabeti, G. W. Stevens, K. A. Mumford, *Chem. Eng. J.* **2024**, *480*, 147934.
[38] R. V. McQuillan, A. Momeni, M. S. Alivand, G. W. Stevens, K. A. Mumford, *Chem. Eng. J.* **2024**, *481*, 148764.
[39] H. Ahn, J. Kim, J.-H. Kim, *Int. J. Greenhouse Gas Control* **2013**, *18*, 165.
[40] G. Liu, W. Jin, *J. Membr. Sci.* **2021**, *636*, 119557.
[41] H. Chamani, J. Woloszyn, T. Matsuura, D. Rana, C. Q. Lan, *Prog. Mater. Sci.* **2021**, *122*, 100843.
[42] H. Anisi, R. V. McQuillan, M. S. Alivand, G. W. Stevens, A. Momeni, O. Mazaheri, K. A. Mumford, *ACS Sustainable Chem. Eng.* **2025**, *13*, 4691.
[43] D. J. Deka, G. G. Jang, A. Kasturi, D. Stamberga, J. K. Keum, R. Custelcean, C. Tsouris, *Sep. Purif. Technol.* **2025**, *354*, 128850.
[44] G. Zotti, S. Zecchin, G. Schiavon, F. Louwet, L. Groenendaal, X. Crispin, W. Osikowicz, W. Salaneck, M. Fahlman, *Macromolecules* **2003**, *36*, 3337.
[45] A. Hartono, I. Kim, H. K. Knuutila, L. V. van der Ham, E. Goetheer, *Energy Procedia* **2017**, *114*, 744.
[46] D. W. Keith, G. Holmes, St. D. Angelo, K. Heidel, *Joule* **2018**, *2*, 1573.
[47] K. Lebling, H. Leslie-Bole, Z. Byrum, L. Bridgwater, https://www.wri.org/insights/direct-air-capture-resource-considerations-and-costs-carbon-removal (accessed: May 2022).
[48] N. McQueen, K. V. Gomes, C. McCormick, K. Blumanthal, M. Pisciotta, J. Wilcox, *Prog. Energy* **2021**, *3*, 032001.
[49] J. F. David Sandalow, C. McCormick, in *ICEF Roadmap*, Innovation for Cool Earth Forum (ICEF), Tokyo, Japan **2018**.
[50] P. S. Kumar, J. A. Hogendoorn, P. H. M. Feron, G. F. Versteeg, *Indus. Eng. Chem. Res.* **2003**, *42*, 2832.
[51] F. Isa, H. Zabiri, N. K. S. Ng, A. M. Shariff, *Int. J. Greenhouse Gas Control* **2018**, *76*, 236.
[52] H. Thee, in *Reactive Absorption of Carbon Dioxide into Promoted Potassium Carbonate Solvents*, University of Melbourne, Department of Chemical and Biomolecular Engineering, Melbourne, Australia **2013**.
[53] H. Thee, K. H. Smith, G. da Silva, S. E. Kentish, G. W. Stevens, *Chem. Eng. J.* **2012**, *181*, 694.
[54] A. F. de Oliveira, *J. Eng. Exact Sci.* **2020**, *6*, 0387.
[55] J. T. Cullinane, G. T. Rochelle, *Fluid Phase Equilib.* **2005**, *227*, 197.
[56] H.-C. Tseng, C.-Y. Lee, W.-L. Weng, I. M. Shiah, *Fluid Phase Equilibria* **2009**, *285*, 90.